Supporting Information

Heterodimers for *in Situ* Plasmonic Spectroscopy: Cu Nanoparticle Oxidation Kinetics, Kirkendall Effect, and Compensation in the Arrhenius Parameters

David Albinsson[1], Sara Nilsson[1], Tomasz J. Antosiewicz[2], Vladimir P. Zhdanov[1,3], and Christoph Langhammer[1]*

[1]Department of Physics, Chalmers University of Technology, 412 96 Göteborg, Sweden

[2]Faculty of Physics, University of Warsaw, Pasteura 5, 02-093, Warsaw, Poland

[3]Boreskov Institute of Catalysis, Russian Academy of Sciences, Novosibirsk 630090, Russia

*clangham@chalmers.se

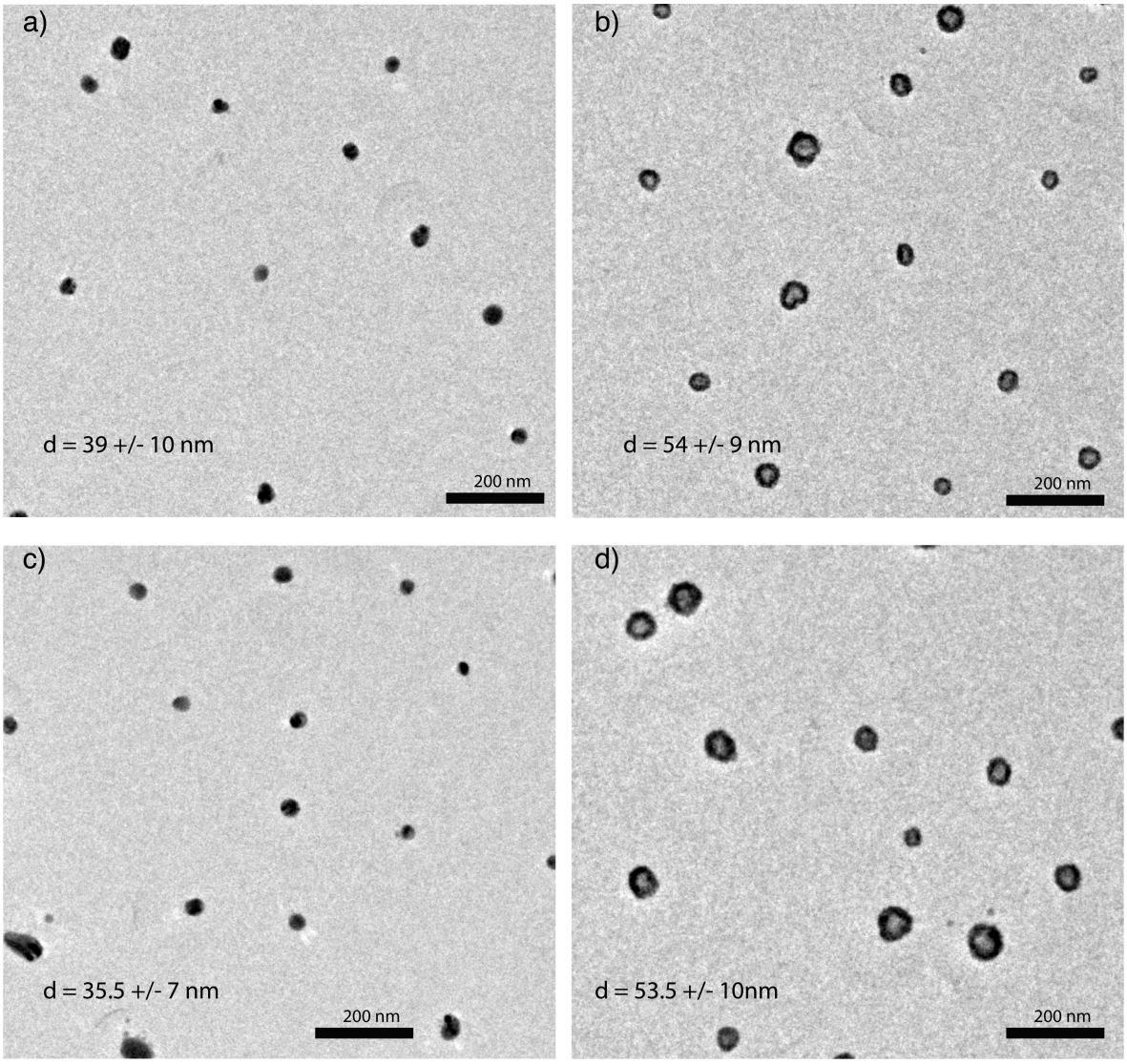

Figure S1. *a) TEM image of Cu nanoparticles that have been reduced in 4% H_2 for 2h at 493 K. b) Same sample after oxidation treatment in 1% O_2 for 1h at 423 K. c) Same sample after a second reduction treatment in 4% H_2 for 2h at 493 K. d) Same sample after second oxidation treatment in 1% O_2 for 1h at 423 K. Clear void formation is seen after repeated oxidation and the Cu particles shrink after reduction to form a solid particle. The indicated diameters are values averaged over a larger sample set of approximately 100 particles for each cycle.*

XPS characterization

Samples were characterized using XPS to verify that the oxide formed during Cu nanoparticle oxidation was mainly Cu_2O and not CuO. The XPS spectra, presented in **Figure S2,** measured on the same sample after initial reduction in 4% H_2 at 493K for 2h, oxidation in 0.5% O_2 at 423 K for 200 s and 1h, respectively. All three curves look very similar and indicate that no CuO has been formed due to the absence of a peak in the 940 – 945 eV range.[1]

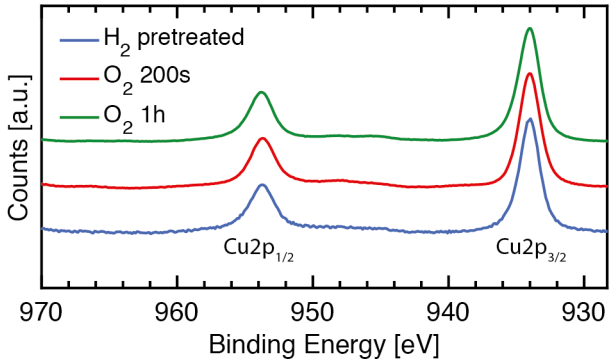

Figure S2*. XPS spectra after reduction and oxidation treatment that confirm the absence of CuO.*

Dielectric functions of porous Cu

To simulate pore formation in the metallic Cu nanoparticle, the Maxwell-Garnett approximation was used to mix the dielectric functions of Cu and vacuum. The corresponding dielectric functions were calculated as:

$$\varepsilon_{Cu-porous}(\beta) = \varepsilon_{Cu}\frac{2(1-\beta)\varepsilon_{Cu} + (1+2\beta)\varepsilon_{pore}}{(2+\beta)\varepsilon_{Cu} + (1-\beta)\varepsilon_{pore}} \qquad (S1)$$

where ε_{Cu} and $\varepsilon_{pore} = 1$ are the dielectric functions of Cu[2] and vacuum, respectively, and β is the volumetric pore fraction. A subset of the dielectric functions obtained in this way is presented in **Figure S3** for pore fractions from 0 to 0.5. Additionally, the red lines show the real and imaginary parts of the bulk metallic Cu dielectric function obtained from the literature.[2]

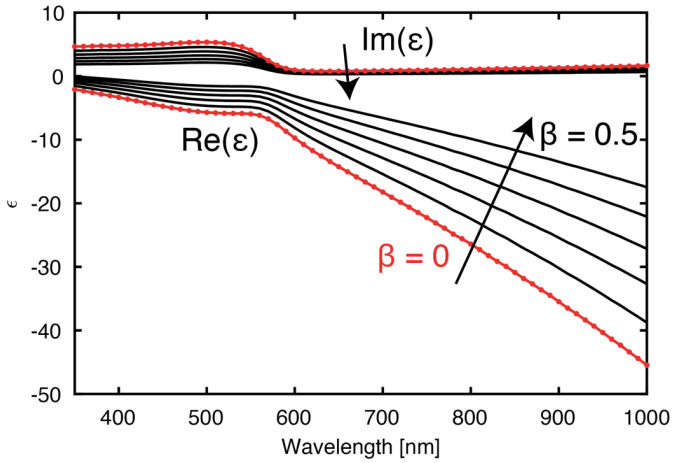

Figure S3. *Dielectric functions for Cu and Cu with voids calculated using eq. S1. Red lines correspond to solid Cu and the black lines to Cu with and increasing void fraction, β, of 0.1, 0.2, 0.3, 0.4 and 0.5.*

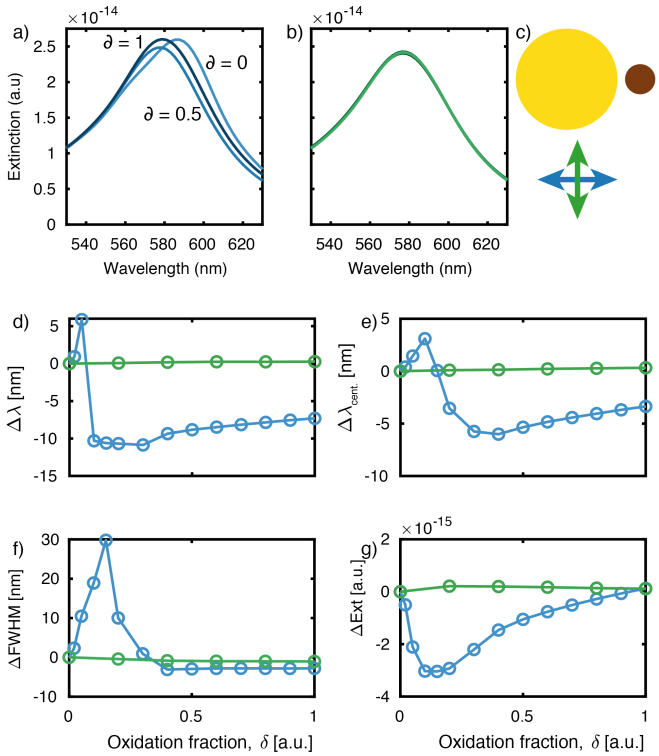

Figure S4. *Polarization dependent optical response to oxidation simulated by FDTD. a) Extinction spectrum evolution for light polarized along the dimer axis for oxidation fractions 0, 0.5 and 1. b) Same as a) for light polarized perpendicular to the dimer axis and showing six simulated spectra for oxidation fractions spanning the range from 0 to 1. c) Schematic depiction of the heterodimer structure used in the simulations. d-g) Extracted peak descriptors* $\Delta\lambda$, $\Delta\lambda_{cent}$, $\Delta FWHM$ *and* ΔExt *from the simulated optical spectra presented as a function of oxidation fraction. Blue lines correspond to light polarized along the dimer axis and green lines to light polarized perpendicular to the dimer axis.*

Benchmarking the FDTD simulation model

To evaluate the influence of changing the simulation geometry on the evolution of the simulated far-field optical response, three model variants were considered. First the influence of moving the Kirkendall hole location inside the Cu nanoparticle was investigated by placing it closer and further away from the adjacent Au disk and by offsetting it perpendicularly to the dimer axis (**Figure S5**). This showed no significant change in the corresponding extinction spectra (**Figure S5a**) and thus we choose a centrally located void in further calculations since in should best represent the average response measured from a large ensemble of particles where the holes are presumed to be randomly distributed.

Alternative oxidation mechanisms were also simulated using the same FDTD scheme as described in the main text. These simulations considered two alternative mechanisms including: (i) coalesced voids located at the metal-oxide interface in the particle with a central metallic core shrinking as the oxidation proceeds (**Figure S6** left), and (ii) That the Cu core gradually becomes increasingly porous all the way to forming a void by using the Maxwell-Garnett mixing model up to 100% porosity (**Figure S6**, right). The comparison of these two models with the model of choice (model 1 in **Figure S6**) indicates that although changing the model quite dramatically, the main characteristics of the optical response is conserved (**Figure S6a-c**). Looking closer at the evolution of the extracted peak parameters, it is also clear that the change in a similar way for all models with some quantitative disagreement to where the corresponding extreme points are found (**Figure S7d,e,f**). From this we note that the characteristic times extracted from our experimental data (**Figure 4**) will be different depending on the model being used to define the points. As a consequence, if the oxidation mechanism is temperature dependent (which we assume it is not in our experimental range), an observed change in kinetic parameters as a function of oxidation fraction could be seen as a result. Thus, we investigated the magnitude such a contribution could have on our Arrhenius analysis by extracting characteristic times using the three models presented in **Figure S6,** followed by Arrhenius analysis using the corresponding characteristic times. This analysis is presented in **Figure S7**, where characteristic times at $\delta =$ 0.5 were extracted from the Extinction data, using the three models, at two temperatures (373K & 423 K). Lines fitted to the most extreme combinations of these points (highest and lowest slope) were then used to find an upper and lower bound of the apparent activation

energy (Text insets lower right of **Figure S7**). From this we see that the variation of E_a is in the order of ± 5 kJ/mole, which is significantly smaller than the observed change in activation energy that is presented in **Figure 4** as a function of oxidation fraction. The same analysis was performed for several values of δ, resulting in the same conclusion.

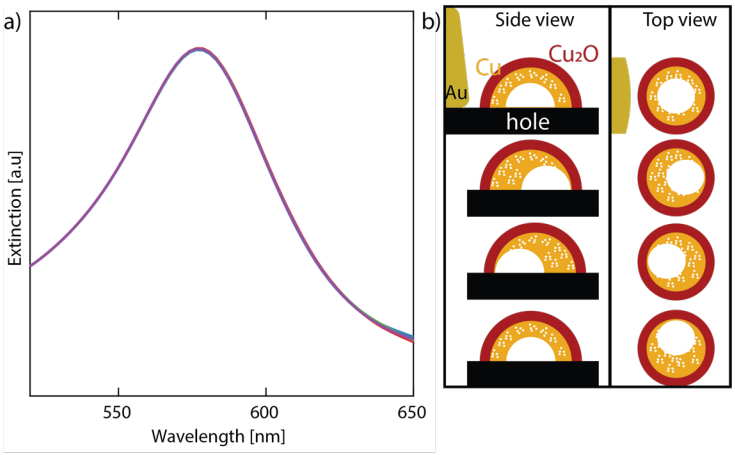

Figure S5. *Effect of changing the location of the Kirkendall hole in the FDTD model. a) four overlaying extinction spectra corresponding to the simulated void positions presented in b). b) Illustration of the four cases showing how the void was shifted in respect to the Au particle shown to the left. All simulations performed at $\delta = 0.5$, a porosity of the metallic Cu of 30 %, and using light polarized along the dimer axis.*

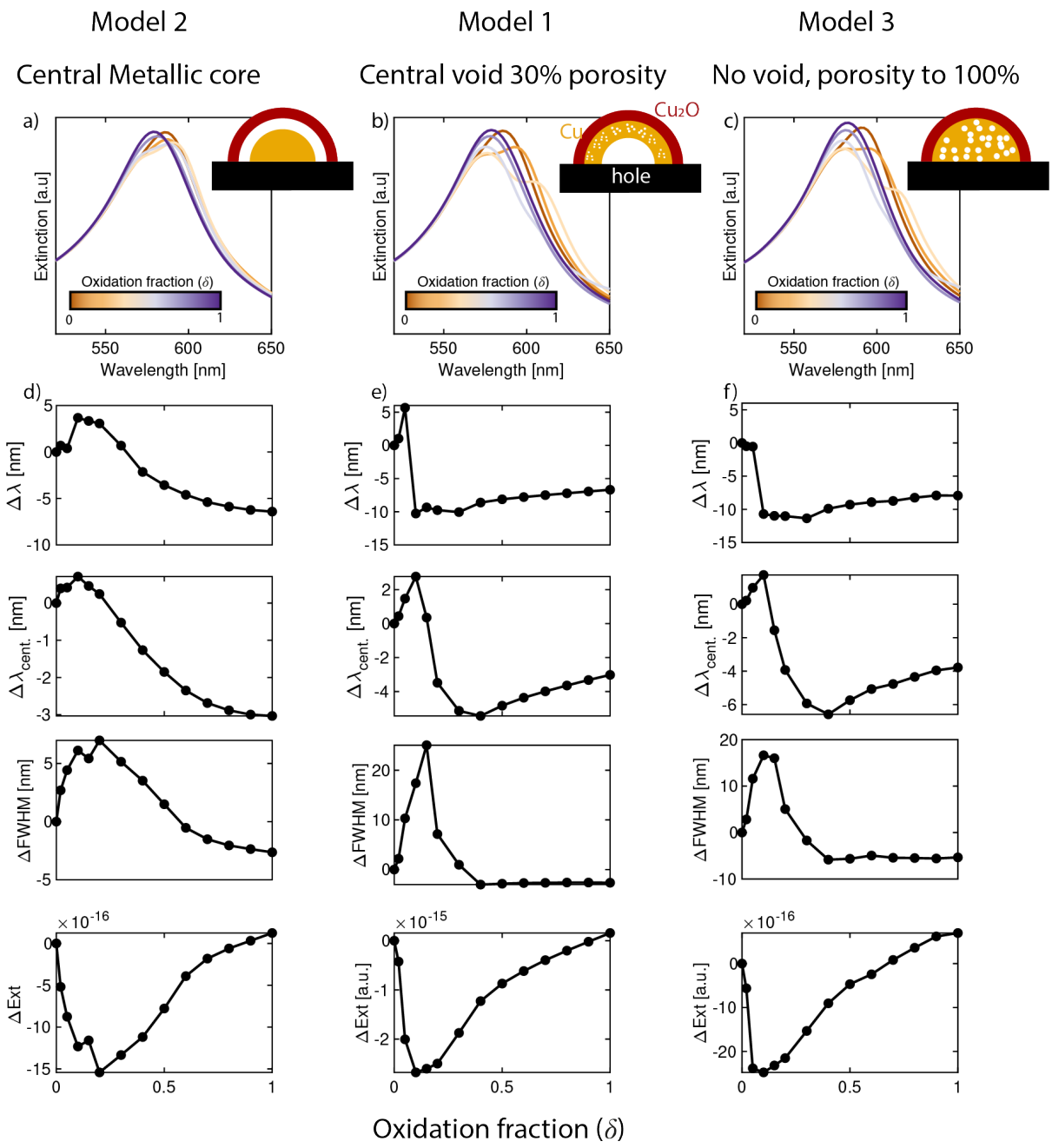

Figure S6. *FDTD simulations of Cu oxidation for three different oxidation models. a-c) Spectral evolution of the plasmon resonance for light polarized along the dimer axis. Insets show illustrations of the corresponding models. The models correspond to (a) voids coalescing at the metal oxide interface leaving a shrinking metallic Cu core, (b) the same model as presented in* ***Figure 3*** *in the main text, and (c) Using the Maxwell-Garnett mixing model all the way to 100% void inclusions making the Cu core gradually more porous. d,e,f) Evolution of the peak parameters extracted using a polynomial fit presented as a function of δ.*

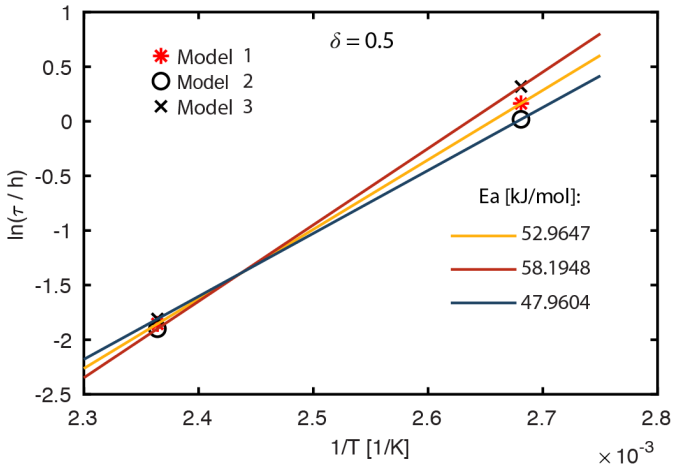

Figure S7. *Arrhenius parameters found using different characteristic times depending on the FDTD model. The markers correspond to* τ *from the three models presented in* ***Figure S7*** *extracted at T = 373 & 423 K. The colored lines correspond to the most extreme slopes (red and blue) and one corresponding to only using points from the model presented in the main text (yellow).*

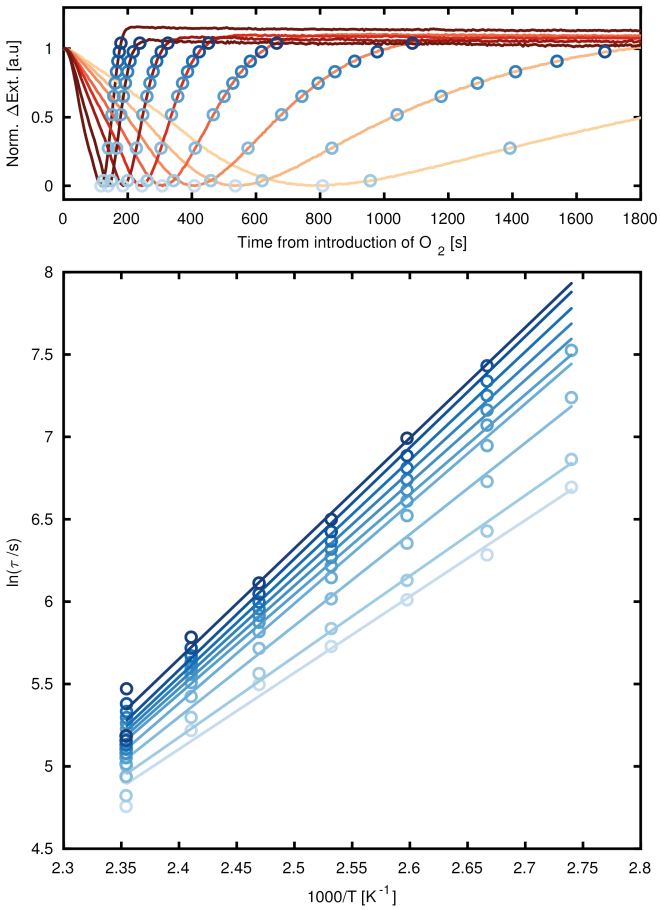

Figure S8. *The top panel shows the same data as in Figure 5 in the main text, with the blue rings corresponding to extracted characteristic times where the extinction value reaches different oxidation fractions. The bottom panel summarizes the corresponding obtained Arrhenius plots used to extract the Arrhenius parameters presented in* ***Figure 6a,b*** *in the main text.*

References

(1) Biesinger, M. C.; Lau, L. W. M.; Gerson, A. R.; Smart, R. S. C. Resolving Surface Chemical States in XPS Analysis of First Row Transition Metals, Oxides and Hydroxides: Sc, Ti, V, Cu and Zn. *Appl. Surf. Sci.* **2010**, *257*, 887–898.

(2) McPeak, K. M.; Jayanti, S. V.; Kress, S. J. P.; Meyer, S.; Iotti, S.; Rossinelli, A.; Norris, D. J. Plasmonic Films Can Easily Be Better: Rules and Recipes. *ACS Photonics* **2015**, *2*, 326–333.